Science and Technology Facilities Council

Technology

Further Characterisation of the Excess-Leakage-Current Effect in HF-CdZnTe using HEXITEC MHz

Ben Cline[a,1], D. Banks[a], M. Bishop[a], A. Davis[a], J. Harris[a], M. Hart[a], S. Knowles[a], T. Nicholls[a], J. Nobes[a], S. Pradeep[a], M. Roberts[a], D. Sole[a], M.C. Veale[a], M.D. Wilson[a], W. Helsby[b] and P. Busca[c]

[a]UKRI STFC Rutherford Appleton Laboratory
[b]UKRI STFC Daresbury Laboratory
[c]ESRF, The European Synchrotron

Email: ben.cline@stfc.ac.uk

30/06/2026

CdZnTe

- **CdZnTe (CZT)**
  - **Widely used in X-ray imaging due to:**
    - High stopping power (>20 keV)
    - Good energy resolution (<1 keV)
    - Room-temperature operation
  - **However, hole trapping and polarization >10^6 ph s^{-1} mm^{-2}**
    - Limits use in advanced medical imaging applications (<10^9 ph s^{-1} mm^{-2})

- **High-Flux CZT (HF-CZT)**
  - Modified growth method designed to improve hole transport properties and reduce these high-flux effects

Aim of this work:
- **Characterise HF-CZT performance at X-ray fluxes >10^6 ph s^{-1} mm^{-2}**
  - **Using 2 mm-thick HF-CZT sensors hybridised to the HEXITEC$_{MHz}$ ASIC**

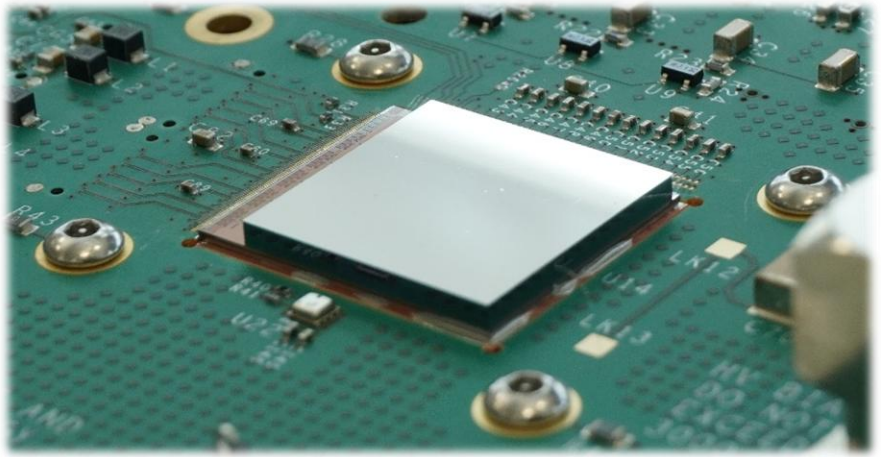

Fig 1: HF-CZT sensor hybridised to the HEXITEC$_{MHz}$ ASIC.

Results from Bishop et al., 2025 [1]

Table 3. Values for mobility and lifetime found from fitting the modified Hecht equation and linear mobility data. *Calculated using the average hole mobility (μ_h) of Detector A-HF,C-HF and D-HF (38 $cm^2V^{-1}s^{-1}$).

Sample	Year Fabricated	$\mu_e\tau_e$ (10^{-3} cm^2V^{-1})	μ_e ($cm^2V^{-1}s^{-1}$)	τ_e (µs)	$\mu_h\tau_h$ (10^{-4} cm^2V^{-1})	μ_h ($cm^2V^{-1}s^{-1}$)	τ_h (µs)
A-HF	2018	5.9	990	6.0	2.4	38	6.2
B-LF	2018	12	840	14.4	0.4	-	1.1*
C-HF	2023	3.4	980	3.5	1.3	44	2.9
D-HF	2023	3.9	790	5.0	1.2	32	3.8

[1] DOI: 10.1088/1748-0221/20/09/P09009

Science and Technology Facilities Council
Technology

Characterisation using HEXITEC$_{MHz}$

- **Fully spectroscopic X-Ray imaging detector (integrating)**
- Capabilities enabling materials characterisation:
  - ✓ **Simultaneous leakage current and photocurrent** readout
  - ✓ **1 MHz** continuous readout (**>10^6 ph s^{-1} mm^{-2}**)
  - ✓ 250 µm (**high spatial resolution)**

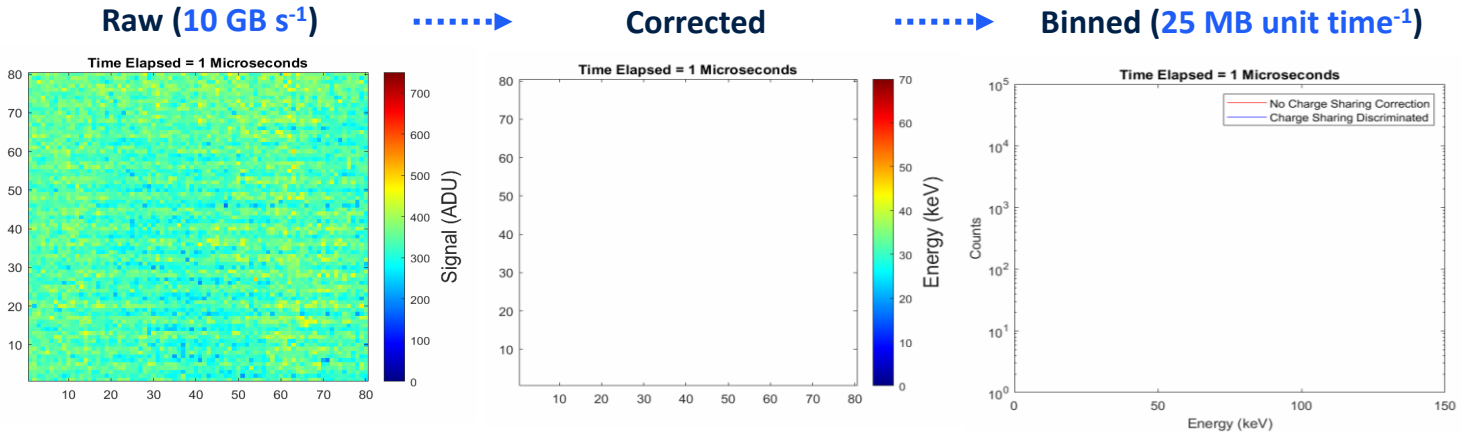

Fig 2: Steps within HEXITEC$_{MHz}$ data pipeline.

Tab 1: Key HEXITEC$_{MHz}$ specifications.

Parameter	Value
Pixel Pitch [µm]	250
Array Size	80 × 80
Max Frame Rate [MHz]	1.0
Max Spectroscopic Flux [ph s^{-1} mm^{-2}]	>10^6
Detector Type	Integrating
Gain Stages [keV in CZT]	100/200/300
FWHM@60keV [keV in CZT]	1.2

Fig 3: The HEXITEC$_{MHz}$ camera system.

Science and Technology Facilities Council

Technology

Initial Characterisation at diamond

- **Diamond Light Source B16 Test Beamline:**
  - Monochromatic **20 keV** X-rays
  - Photon fluxes: 10^5 – 10^7 ph s^{-1} mm^{-2}
  - Tested **HF-CZT (2 mm)**, p-type Si (300 µm) devices

- **600 s dynamic measurements with periods of irradiation and detector recovery**

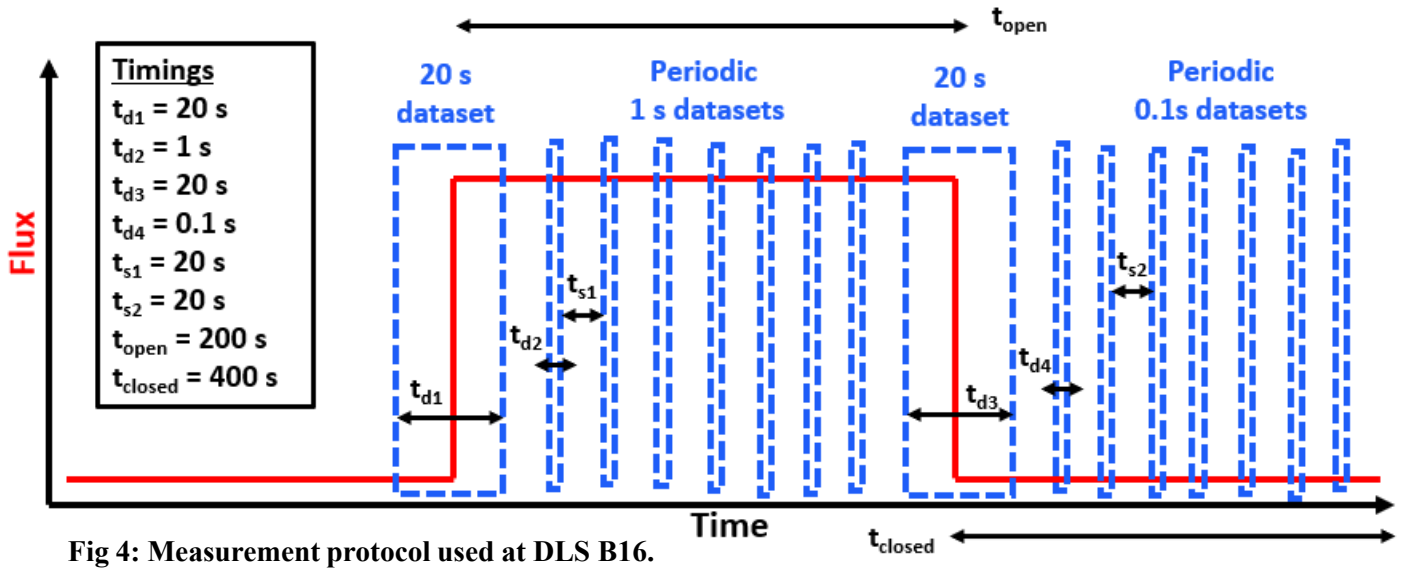

Fig 4: Measurement protocol used at DLS B16.

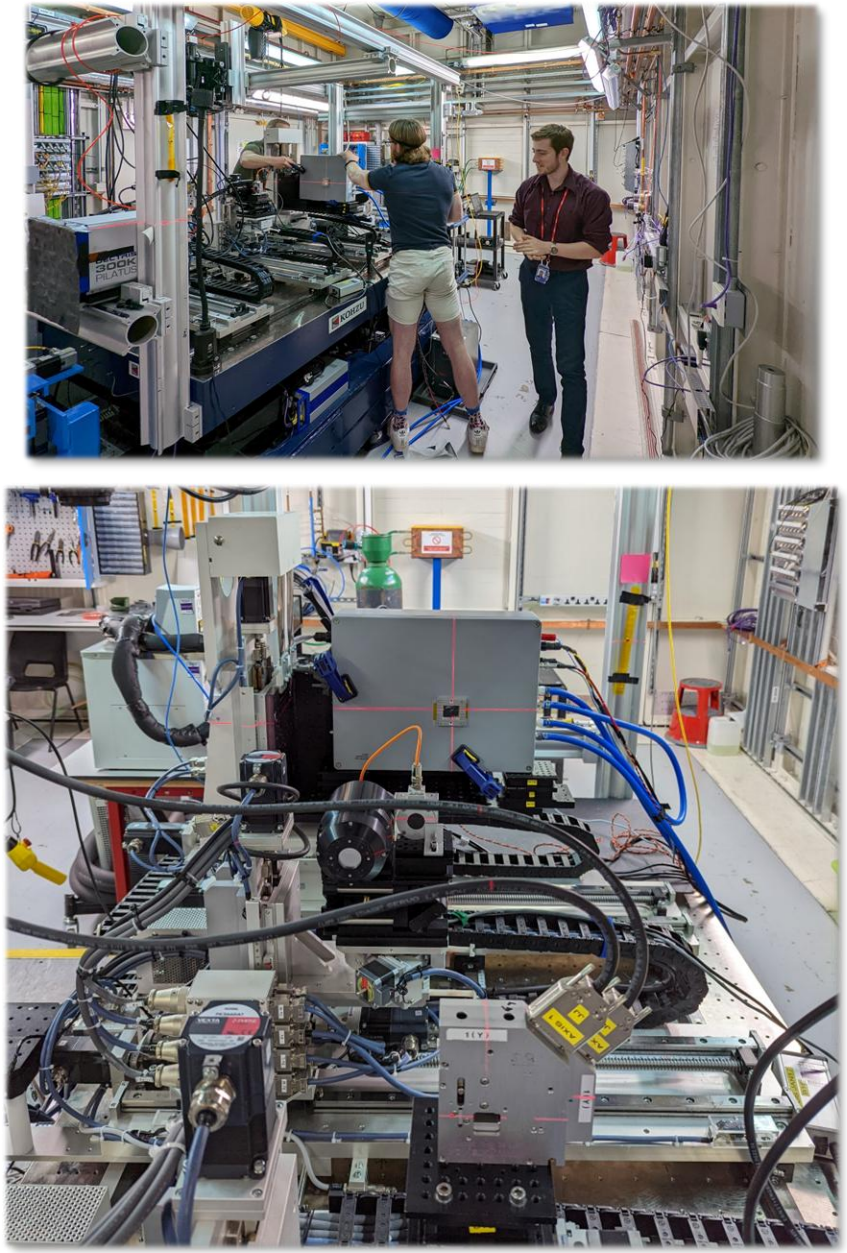

Fig 5: B16 setup photos.

Science and Technology Facilities Council
Technology

DOI: 10.1088/1748-0221/19/04/P04028

DOI: 10.1088/1748-0221/20/10/P10021

Identification of ‘excess-leakage-current’ effect

Baseline shift of irradiated pixels towards higher digital values, indicative of excess leakage current generation

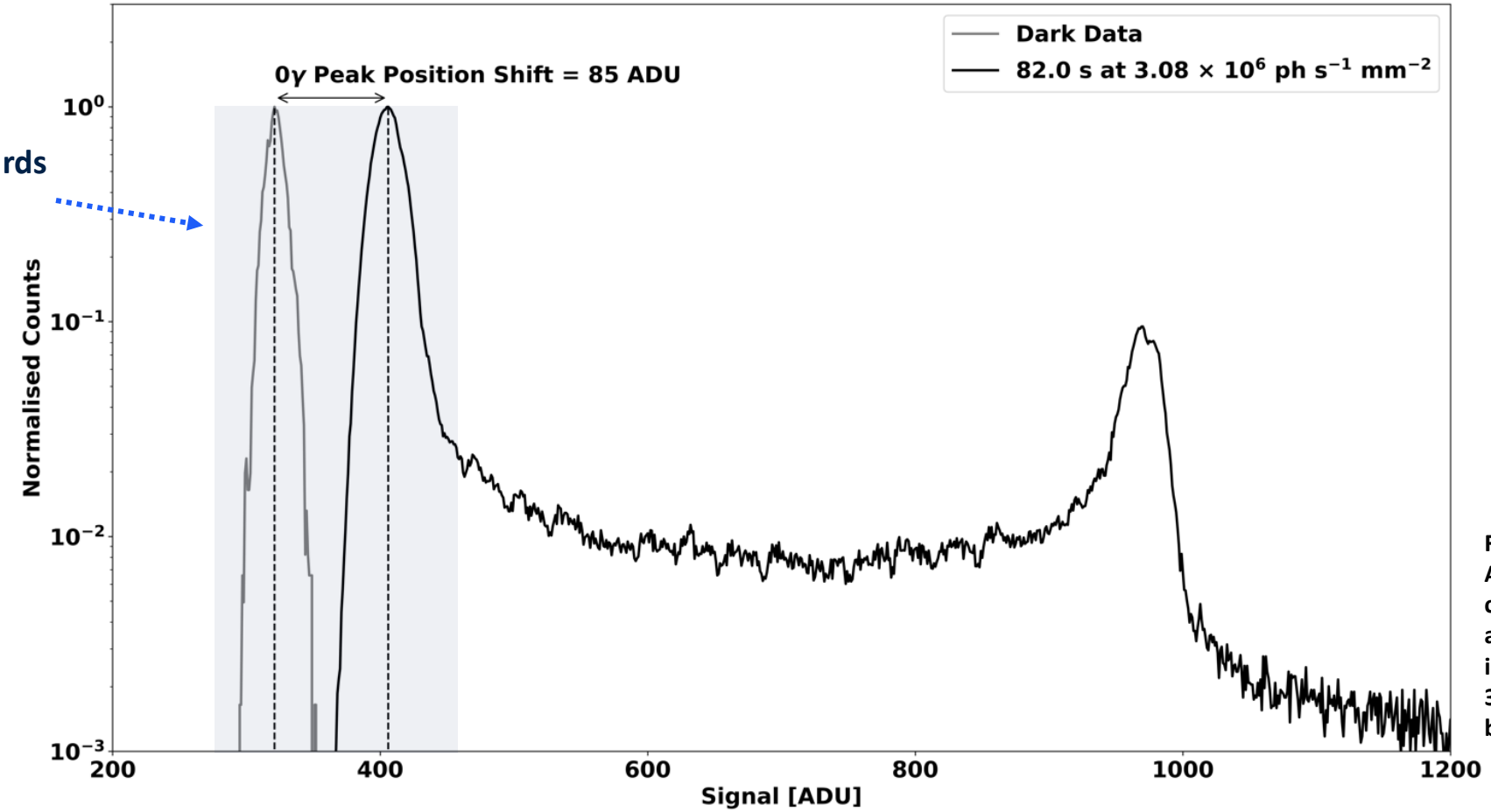

Fig 6: Min-max normalised ADU spectra of a single pixel captured without irradiation and following 82 s of irradiation at a 20 keV flux of 3.08×10^6 ph s^{-1} mm^{-2} – 1 ADU bin width.

Intrinsic to HF-CZT – does not occur in p-type Si

Science and Technology Facilities Council

Technology

Identification of ‘excess-leakage-current’ effect

Baseline shift of irradiated pixels higher digital val indicative of exc leakage current generation

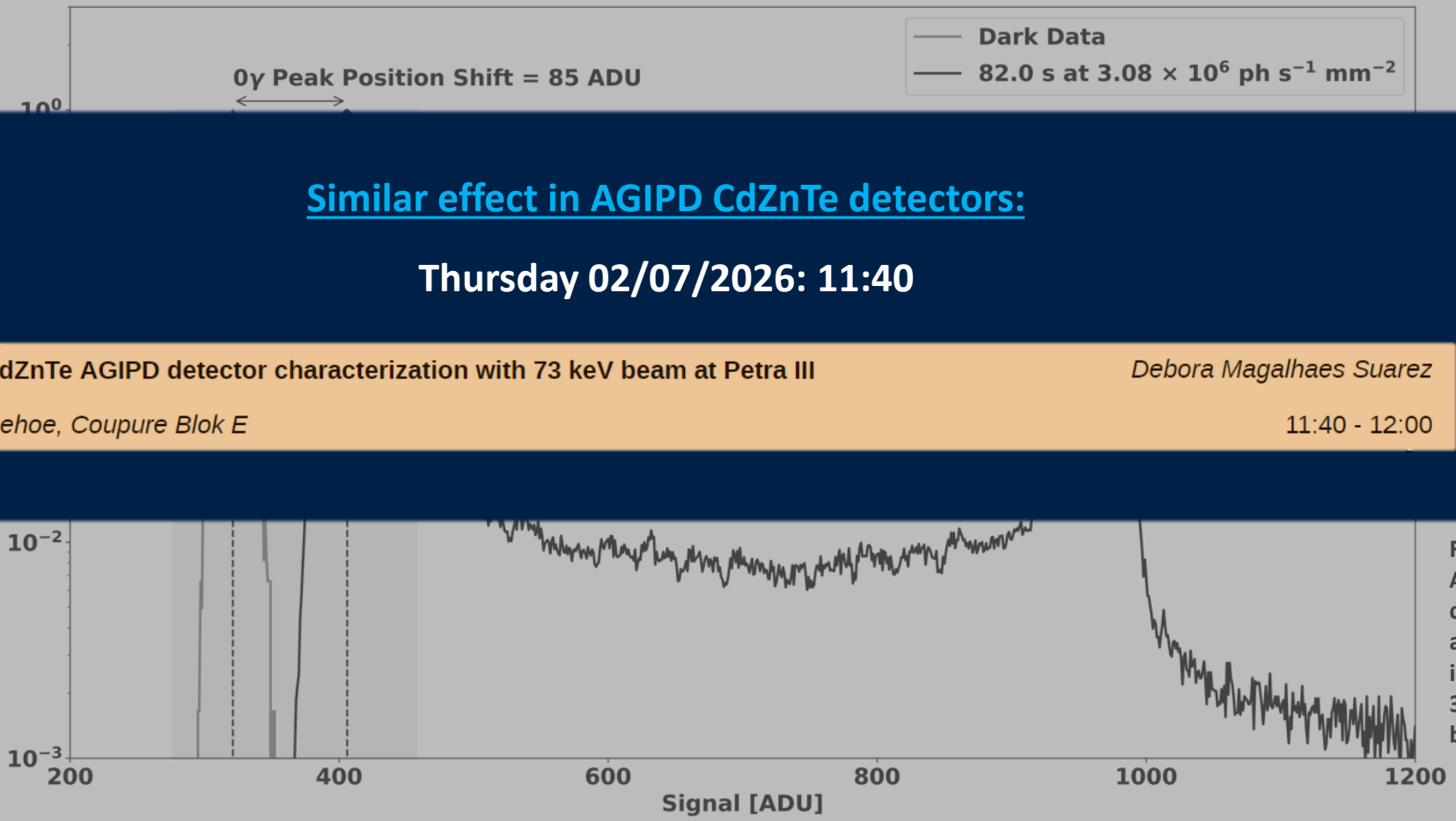

Similar effect in AGIPD CdZnTe detectors:

Thursday 02/07/2026: 11:40

CdZnTe AGIPD detector characterization with 73 keV beam at Petra III	*Debora Magalhaes Suarez*
Oehoe, Coupure Blok E	11:40 - 12:00

Fig 6: Min-max normalised ADU spectra of a single pixel captured without irradiation and following 82 s of irradiation at a 20 keV flux of 3.08×10^6 ph s^{-1} mm^{-2} – 1 ADU bin width.

Intrinsic to HF-CZT – does not occur in p-type Si

Science and Technology Facilities Council

Technology

Dynamics of effect

1. Immediate generation of excess current upon irradiation

2. Gradual rise in excess current throughout irradiation towards steady-state value

3. Non-instantaneous recovery following irradiation – excess current decays over extended period

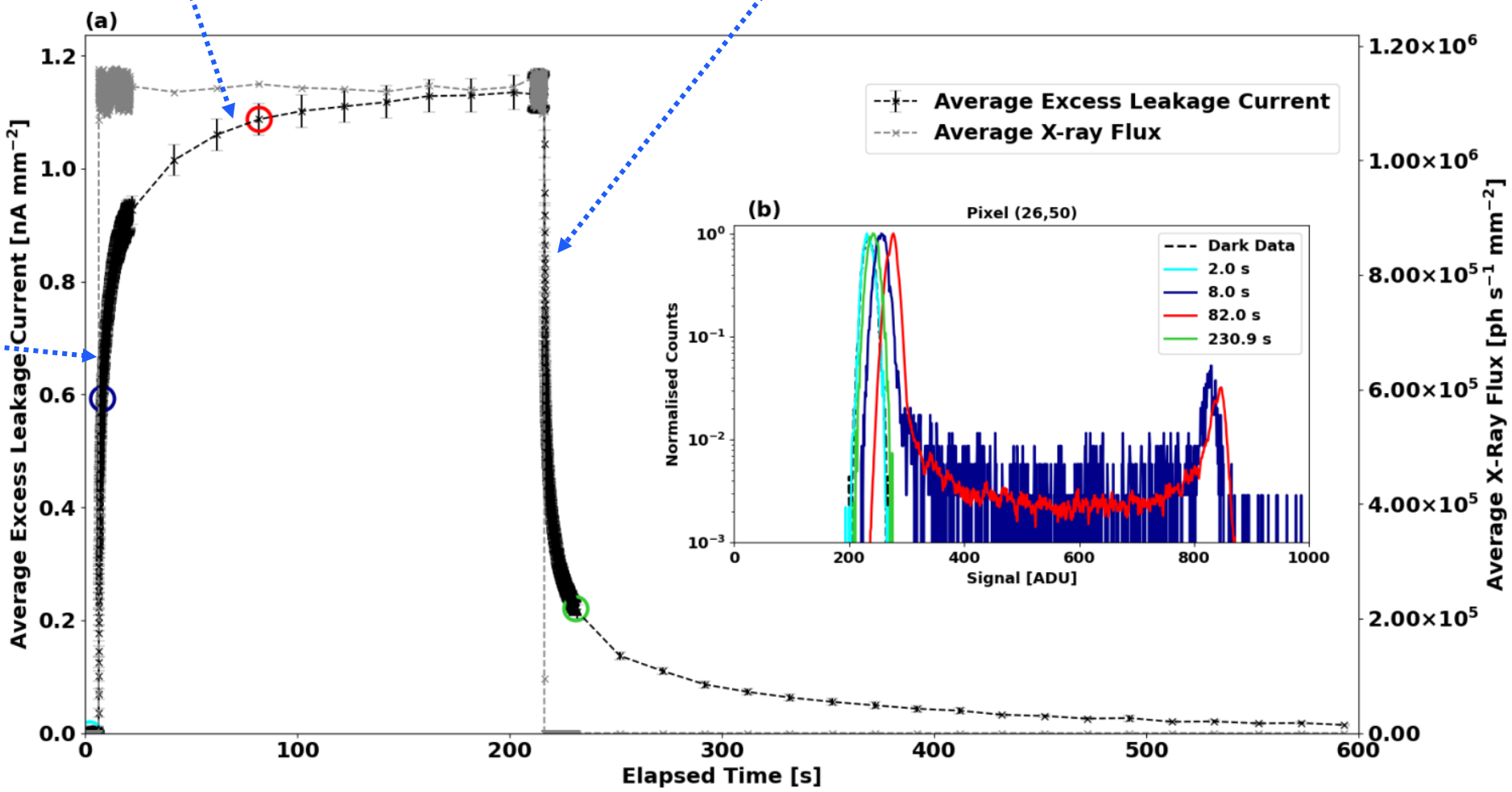

Fig 7: (a) Excess leakage current (black) and X-ray flux (grey) measured during a 20 keV irradiation using 6.5 mm of Al attenuation. (b) Min-max normalised raw single-pixel spectra obtained at four chosen times – 1 ADU bin width.

Science and Technology Facilities Council
Technology

Dynamics of effect

1. Immediate generation of excess current up[on] irradiation

2. Gradual rise in excess current throughout irradiation towards steady-state value

3. Non-instantaneous recovery following irradiation – excess current decays over extended period

Why is this important?

- Reduces detector's dynamic range (max measurable energy)
- Time-dependent detector performance

→ **Both affect an end user of the detector if unaccounted for**

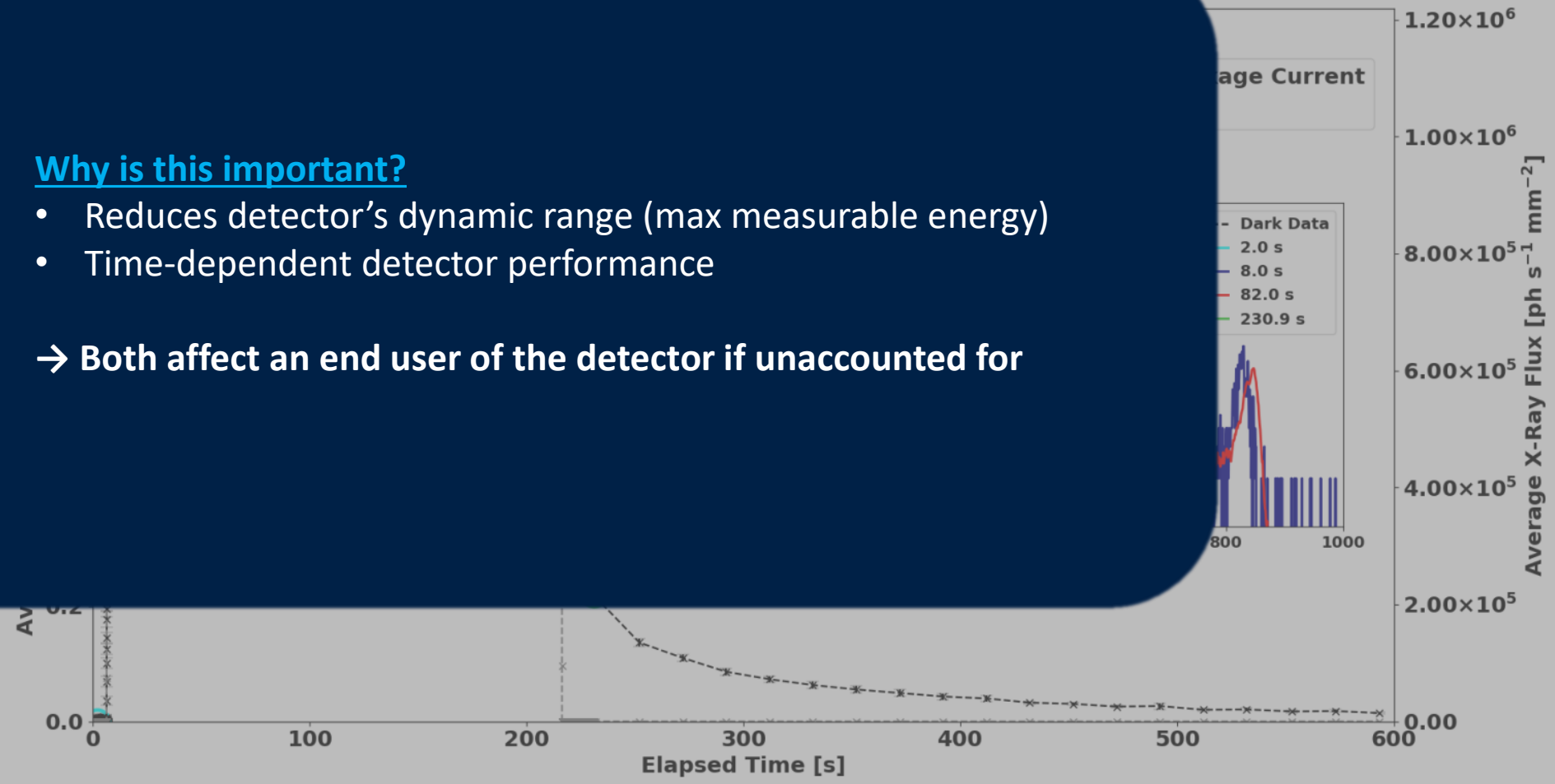

Fig 7: (a) Excess leakage current (black) and X-ray flux (grey) measured during a 20 keV irradiation using 6.5 mm of Al attenuation. (b) Min-max normalised raw single-pixel spectra obtained at four chosen times – 1 ADU bin width.

Science and Technology Facilities Council

Technology

Investigating its origin

Spatial Dependence

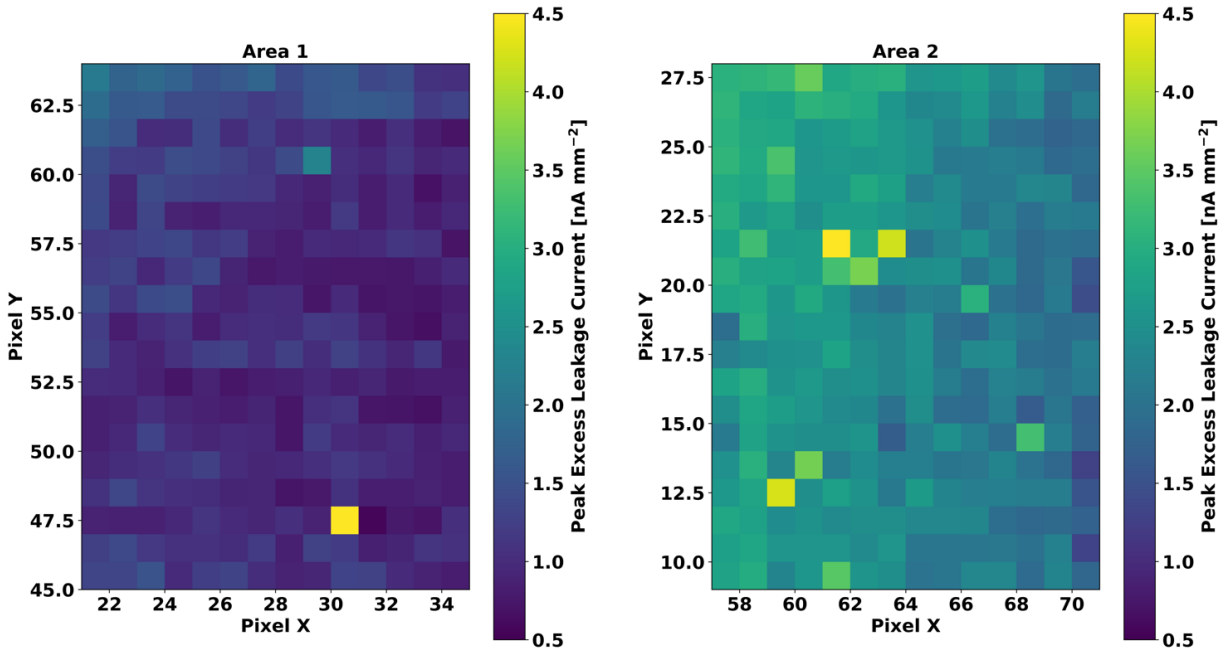

Fig 8: Spatial dependence of phenomenon.

Device-wide spatial variation indicates **intrinsic material effect**

Correlation with energy resolution

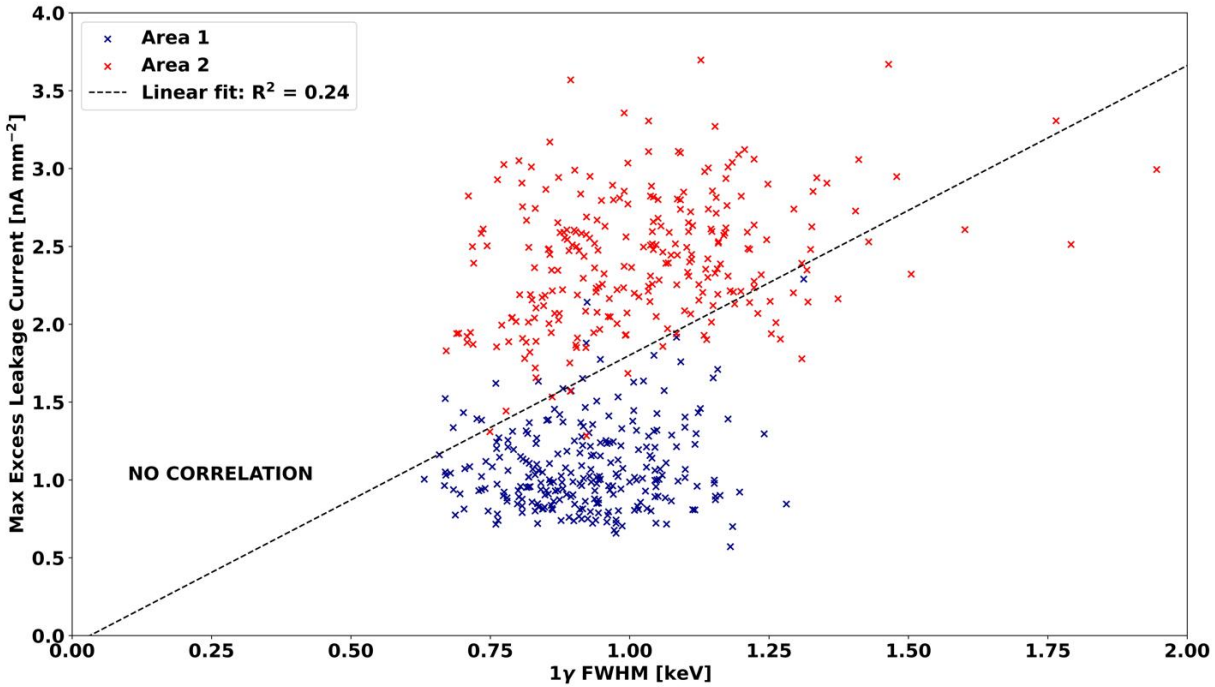

Fig 9: Correlation between the excess leakage current and the energy resolution.

Absence of correlation indicates **surface-related phenomenon**

Science and Technology Facilities Council

Technology

Investigating its origin

Temperature dependence

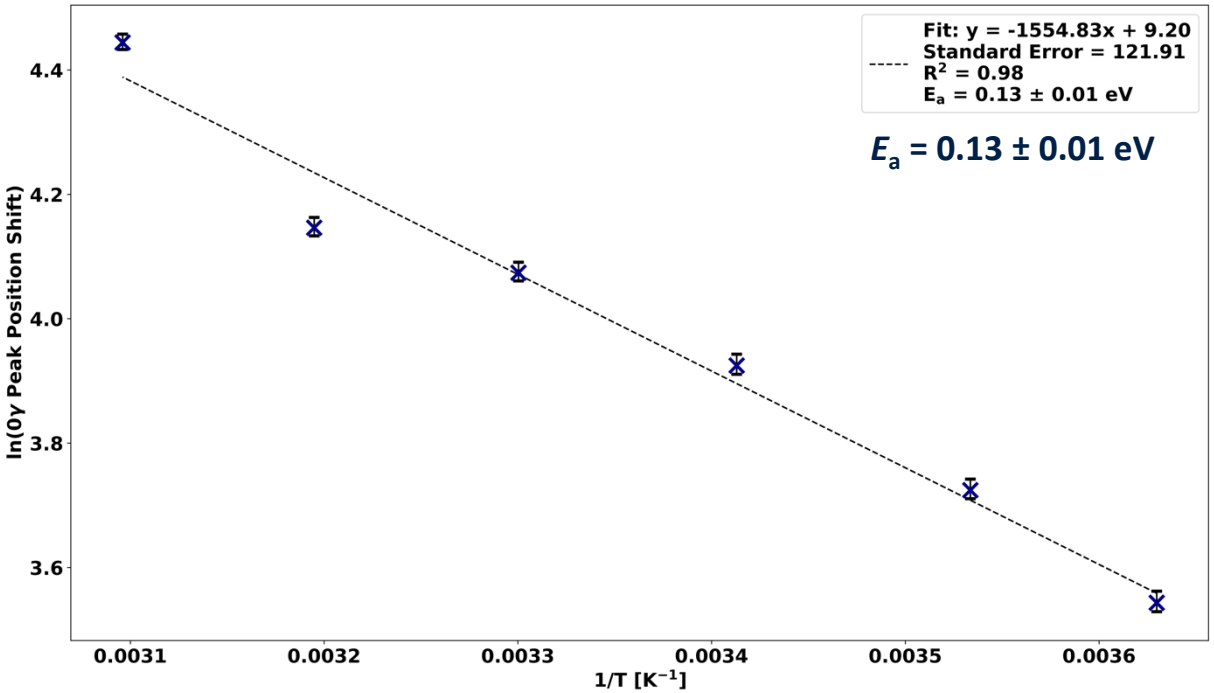

Fig 10: Temperature dependence (Arrhenius analysis) of phenomenon.

Calculated E_a consistent with well-documented Cd-related defects

Intensity dependence

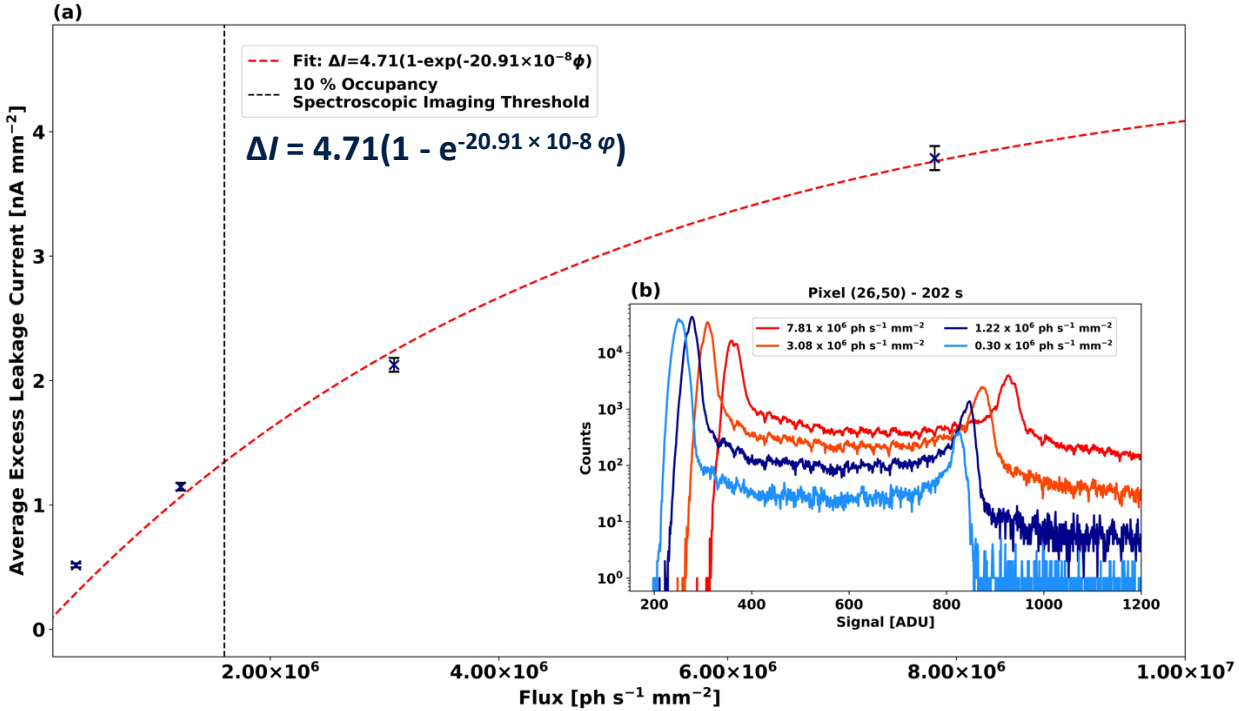

Fig 11: Intensity dependence of phenomenon.

Flux-dependent measurements indicate saturation at high intensities

Science and Technology Facilities Council
Technology

Investigating its origin

Temperature dependence

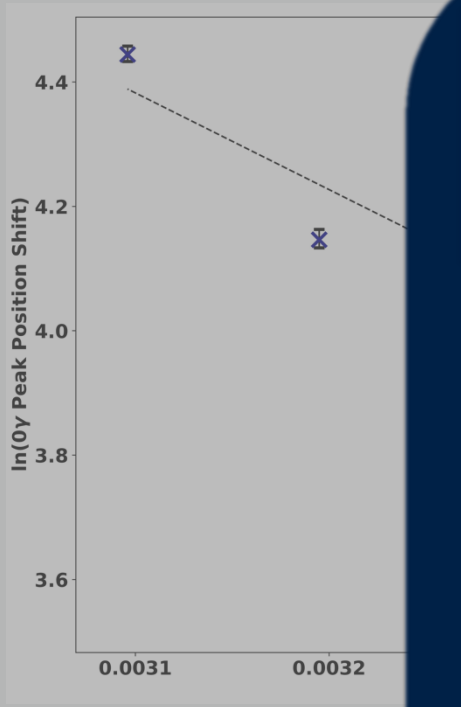

Fig 10: Temperature deper

Calculated E_a consis

Intensity dependence

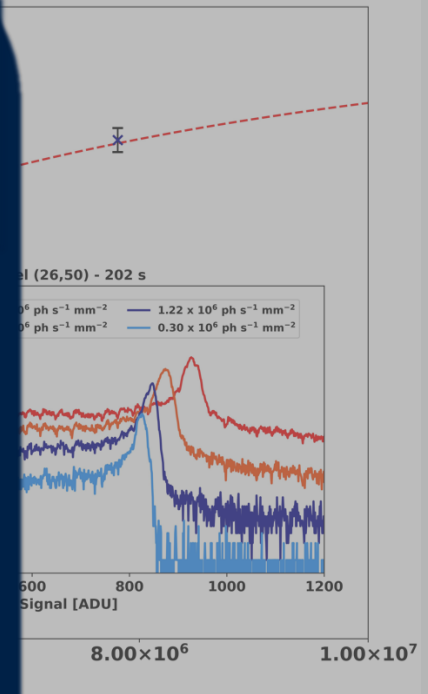

ion at high intensities

Initial Hypothesis: Anode-based effect

- Photoelectron trapping at Cd acceptor states near the anode–CZT interface
- Accumulated space charge modifies potential barrier, altering the leakage current
- Effect saturates when all available traps are filled or when the anode barrier is fully reduced, leading to recombination-limited behaviour

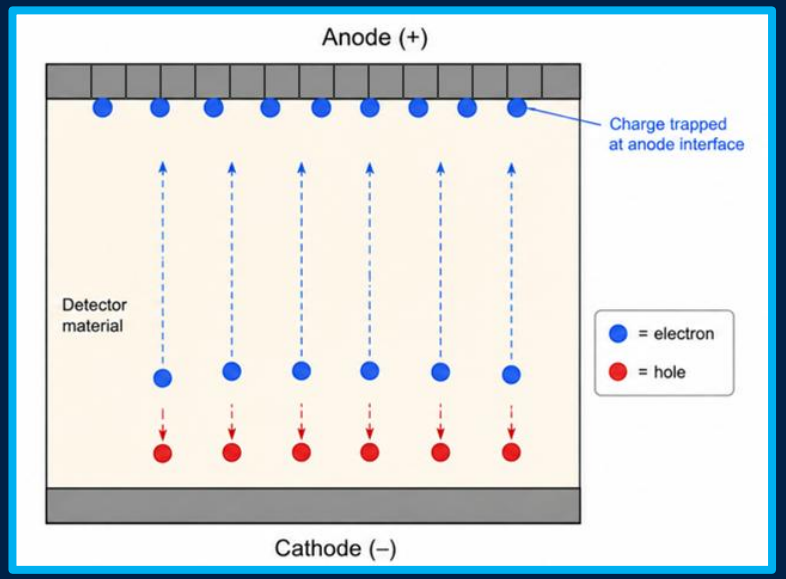

Fig 12: Schematic of proposed anode effect.

Science and Technology Facilities Council

Technology

Further characterisation at ESRF

The European Synchrotron

- **ESRF BM05 beamline:** extended measurements beyond DLS B16 conditions
  - Higher photon energies: **50 keV, 70 keV**
  - Higher flux range: 10^5–10^8 ph s^{-1} mm^{-2}

- **Measurement protocol based on that used at DLS**

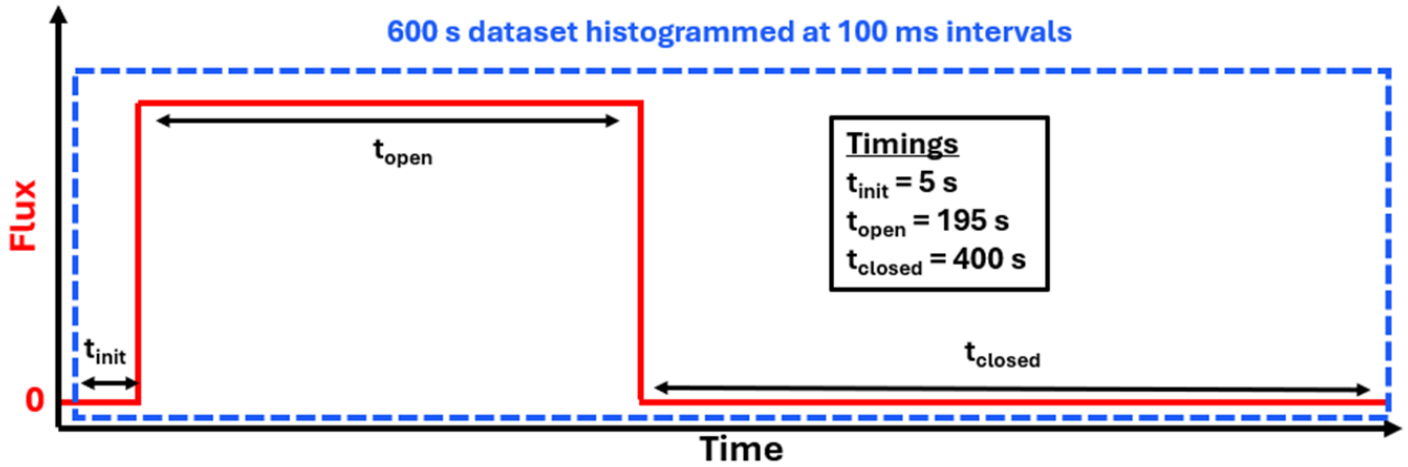

Fig 13: Measurement protocol used at ESRF BM05.

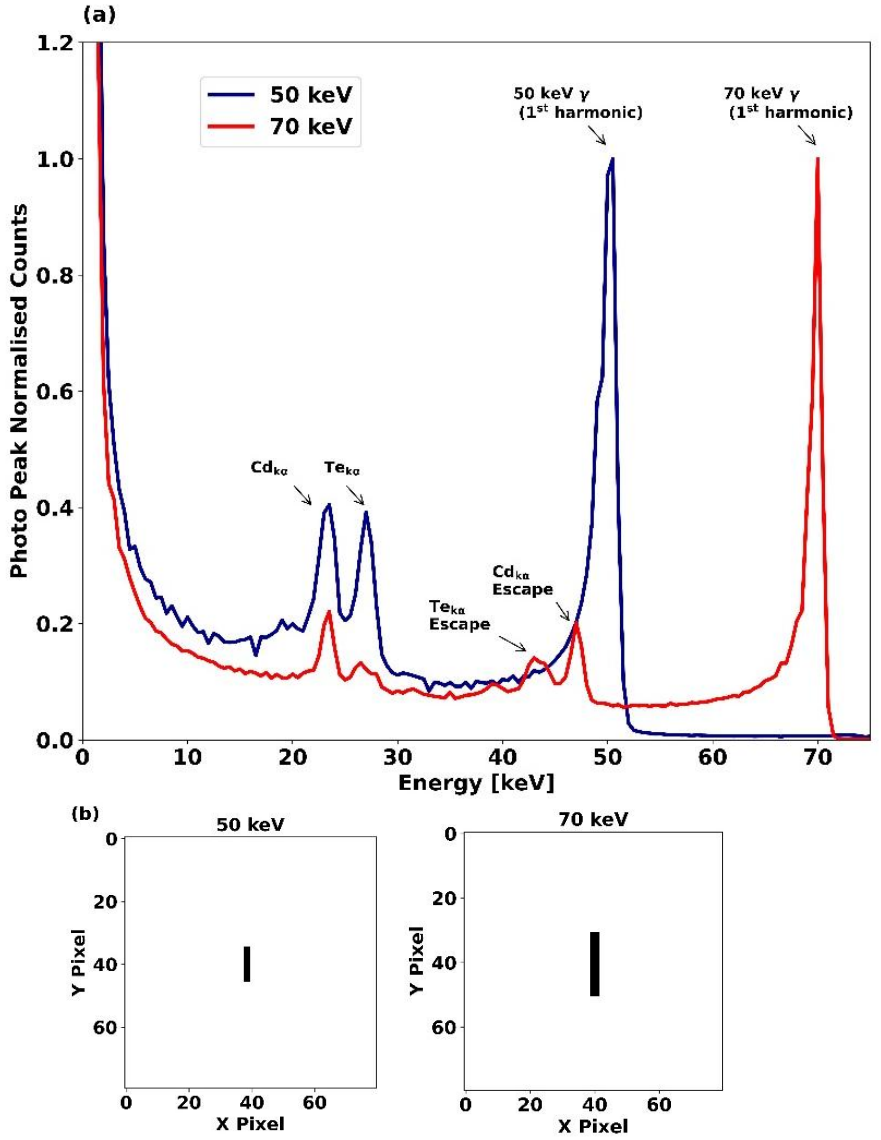

Fig 14: Global normalised spectra of illuminated pixels in 50 keV (7.5×10^5 ph s^{-1} mm^{-2}) and 70 keV (5.7×10^4 ph s^{-1} mm^{-2}) datasets.

UKRI Science and Technology Facilities Council

Technology

Investigating its origin

Energy Dependence

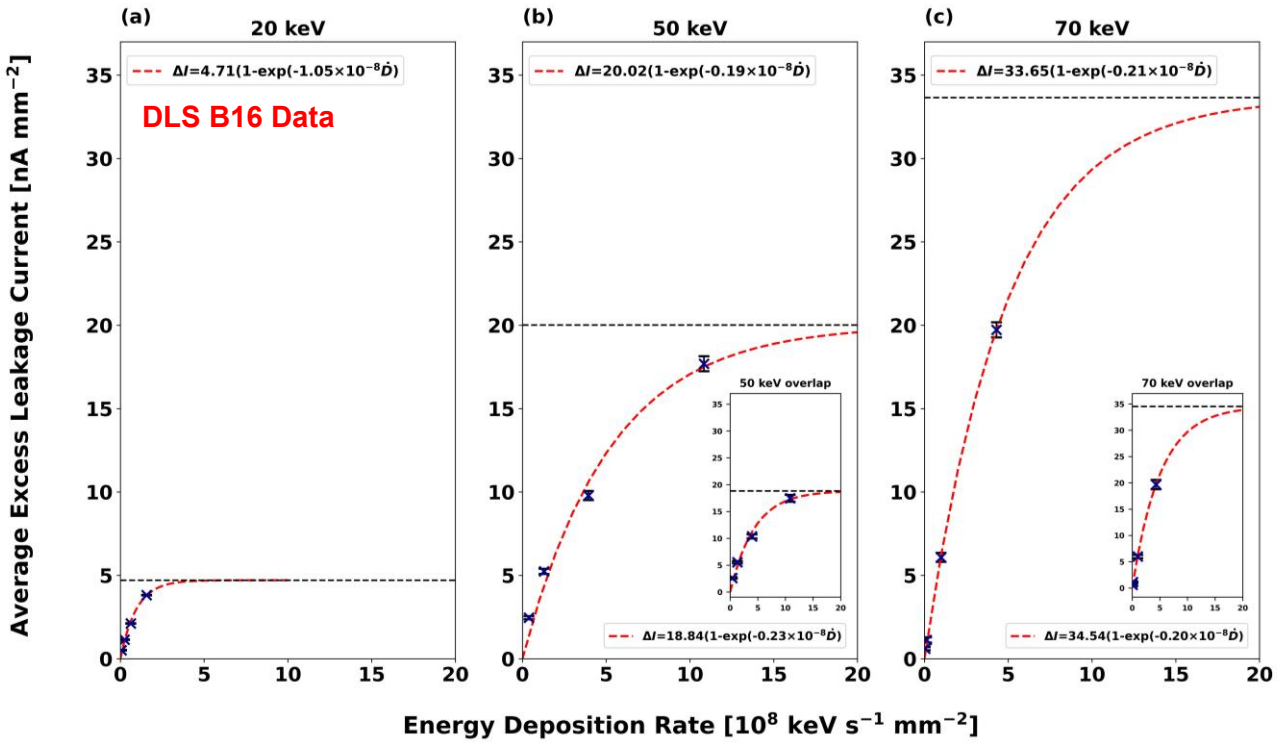

Fig 15: Energy dependence of phenomenon.

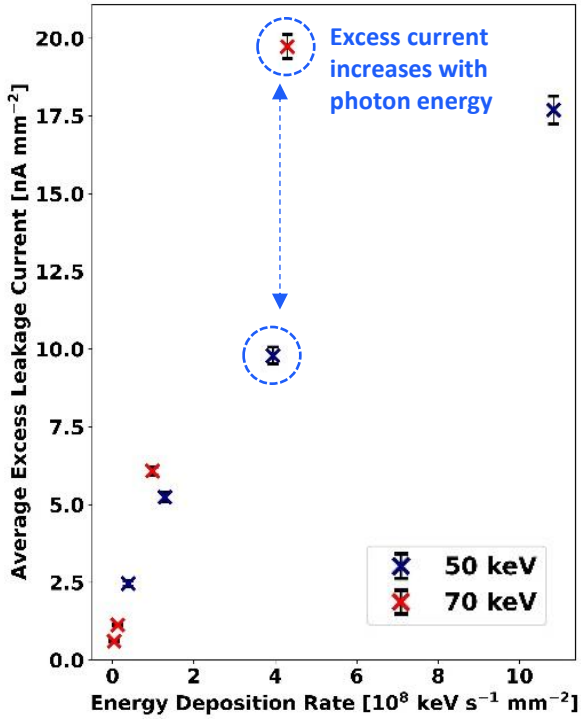

Fig 16: Energy dependence of phenomenon.

Higher saturation currents at higher energies suggest **non-anode-only mechanism**

Excess current increases with energy (constant EDR), indicating **DOI dependence**

Science and Technology Facilities Council

Technology

Investigating its origin

Energy Dependence

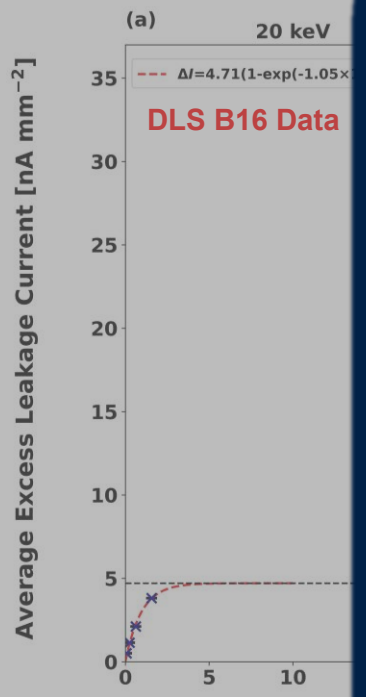

Fig 15: Energy depe

Higher saturat

Amended Hypothesis: Dual Anode-Cathode Mechanism

- **Low energies**:
  - Photoelectron trapping in acceptor states at anode dominates
- **Higher energies**:
  - Increased interaction depth enhances hole trapping near cathode
  - Anode space charge reduces bulk electric field, enhancing hole trapping
  - Trapped holes induce cathode response analogous to that anode
- Effect saturates when all available traps are filled or both contact barriers are fully reduced, leading to recombination-limited behaviour.

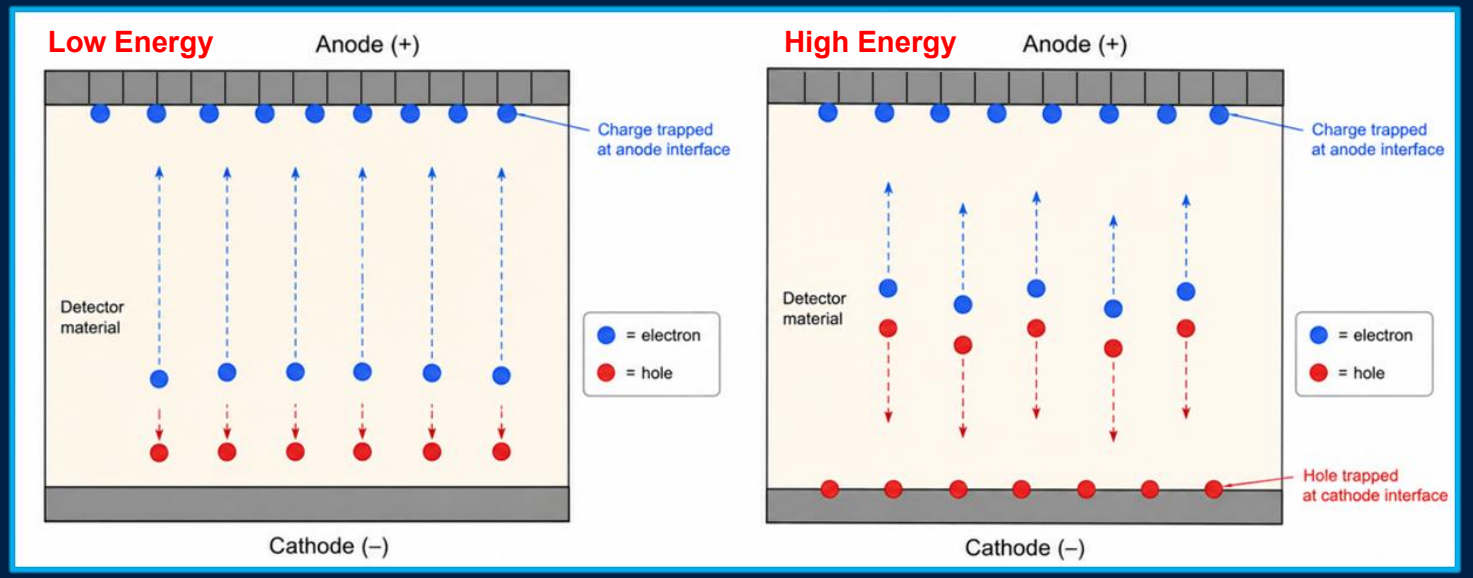

Fig 17: Schematic of proposed dual anode-cathode mechanism.

energy (constant EDR),

enon.

Science and Technology Facilities Council

Technology

A solution? High-Flux CZT with a new contact configuration

New Anode Contact

REDLEN TECHNOLOGIES

- Key Changes
  - Anode: Pt → Ti/Au
    - Improved short term count stability
    - Improved leakage current stability over a temperature range
    - Thicker metallization for better FCB (solder or CE)
  - Encapsulation: None → SU-8
    - Provides protection for streets and pixels for attachment
  - Sensor Thickness: 2mm → 1.5mm
    - More balanced pixel pitch/thickness aspect ratio - reduces charge sharing
    - Allows lower bias voltage of -500 to -700 Vdc

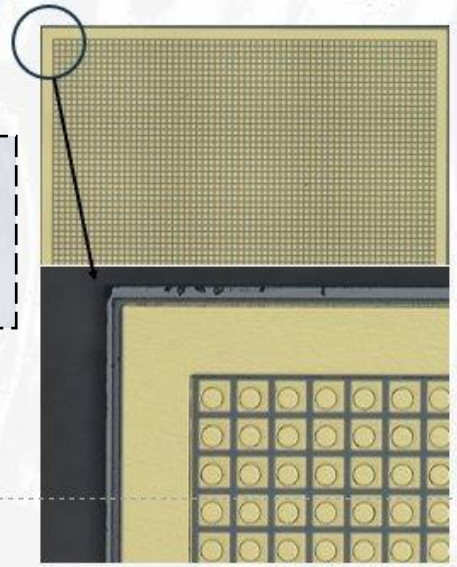

WORK OF REDLEN TECHNOLOGIES

12

Presented at HiZPAD '25

https://indico.esrf.fr/event/172/contributions/1106/

Fig 18: HiZPAD '25 slide presented by Redlen Technologies.

Science and Technology Facilities Council

Technology

A solution? High-Flux CZT with a new contact configuration

New Anode Contact

- Ti/Au + SU-8 shows a more square current waveform and better current stability at higher temperature
- Ti/Au + SU-8 shows slightly fewer counts than Pt, similar count waveform as Pt

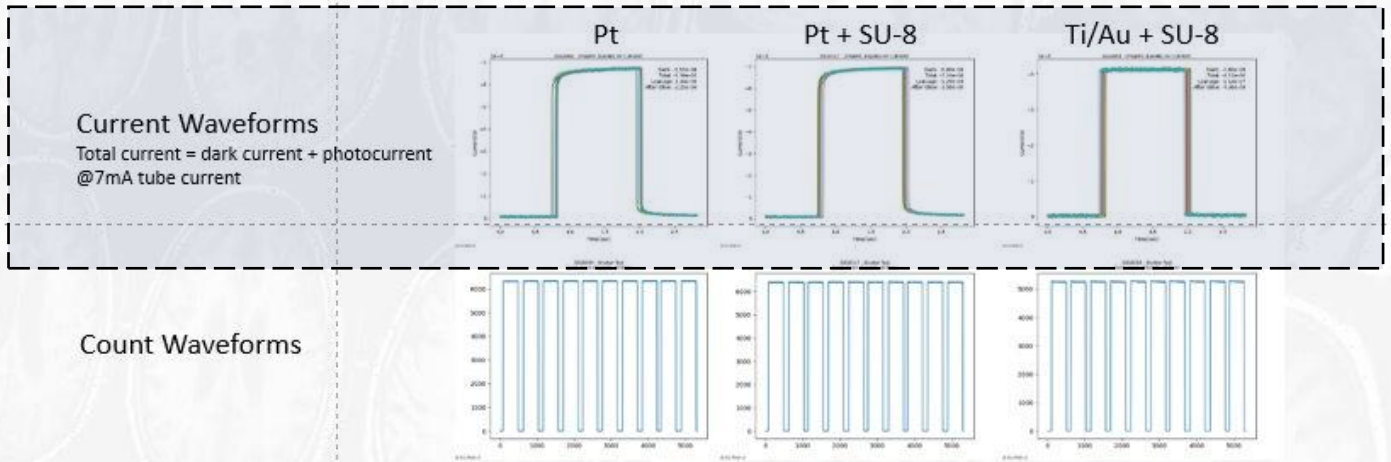

WORK OF REDLEN TECHNOLOGIES

13

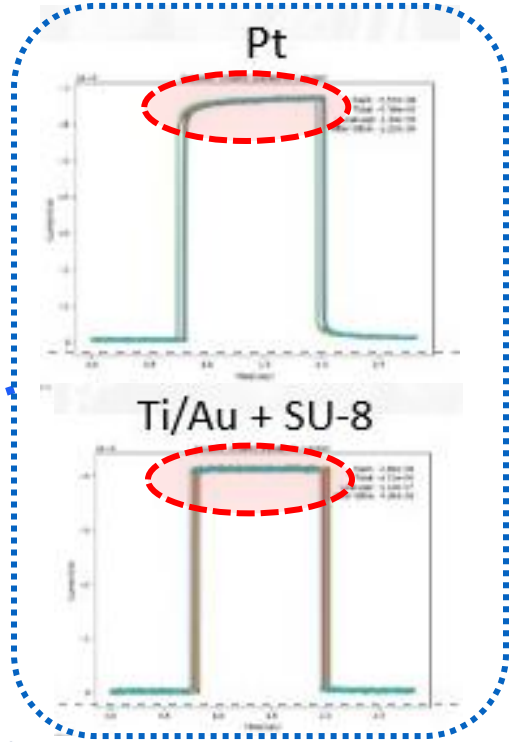

Presented at HiZPAD '25

https://indico.esrf.fr/event/172/contributions/1106/

Fig 19: HiZPAD '25 slide presented by Redlen Technologies.

Science and Technology Facilities Council

Technology

CZT device comparison at Science and Technology Facilities Council Technology

- To investigate the effect of contact technology, **three CZT detector variants were evaluated**
- **Primary differences** between devices are:
  - **Conductivity type** (n-type/p-type)
  - **Φ_m** (contact metal work function)

Tab 2: Overview of CZT devices tested.

Name	Variant	Electrodes	Conductivity Type	Thickness [mm]	Φ_m [eV]
HF-1	HF-CZT	Pt/CdZnTe/Pt	P-type	2.0	5.65
HF-2	HF-CZT	Pt/CdZnTe/Ti/Au	P-type	2.0	5.65 / 4.33
LF-1	LF-CZT	Pt/CdZnTe/Pt	N-type	2.0	5.65

- Measurements utilised:
  - **Mo fluorescence** using a 160 kVp, 30 mA W X-ray tube
    - **Easy access (laboratory-based system)**
    - **Polychromatic source (vs. synchrotron monochromatic beam)**

* Calculated using thresholds of 0γ + 200 ADU

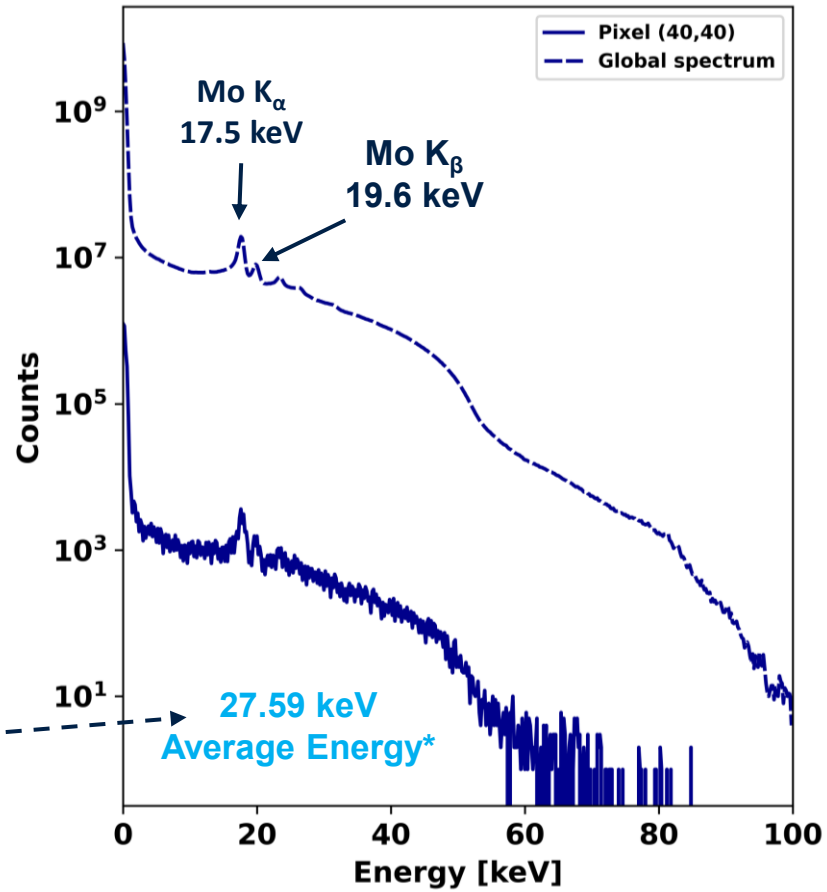

Fig 20: HEXITEC$_{MHz}$ fluorescence spectrum measured using a W X-ray tube at 60 kV.

Science and Technology Facilities Council Technology

Mo fluorescence: excess leakage current measurements

- Fluxes: **10^5 - 10^7 ph s^{-1} mm^{-2}**

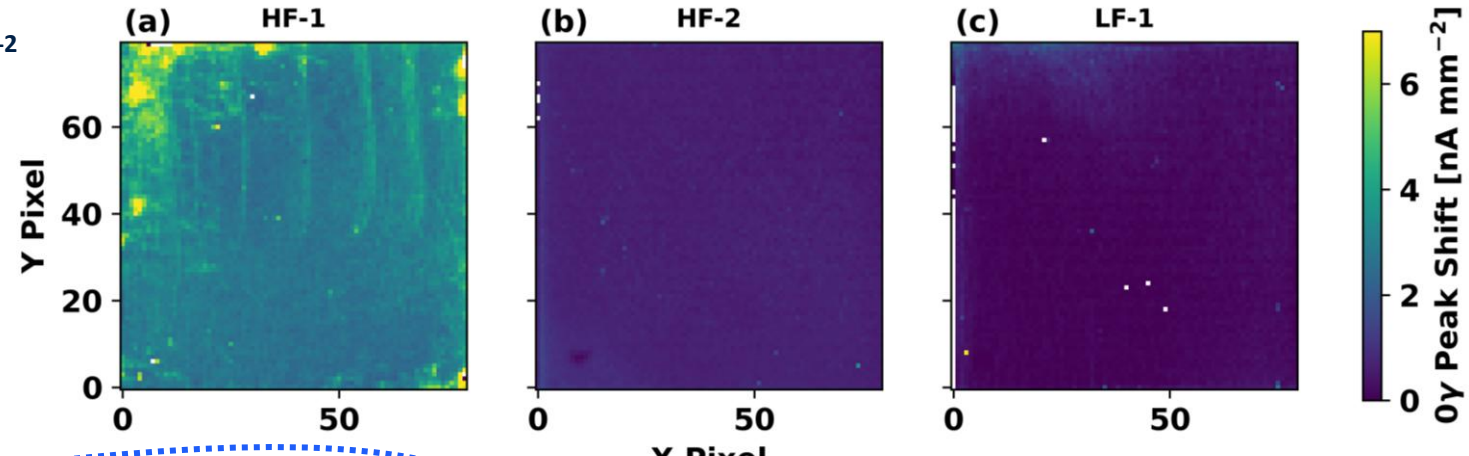

Fig 21: Excess leakage current measured in each device at ~7 × 10^6 ph s^{-1} mm^{-2}.

1. Lower Ti/Au ϕ_m cf. Pt
→ higher anode barrier
→ lower excess leakage current

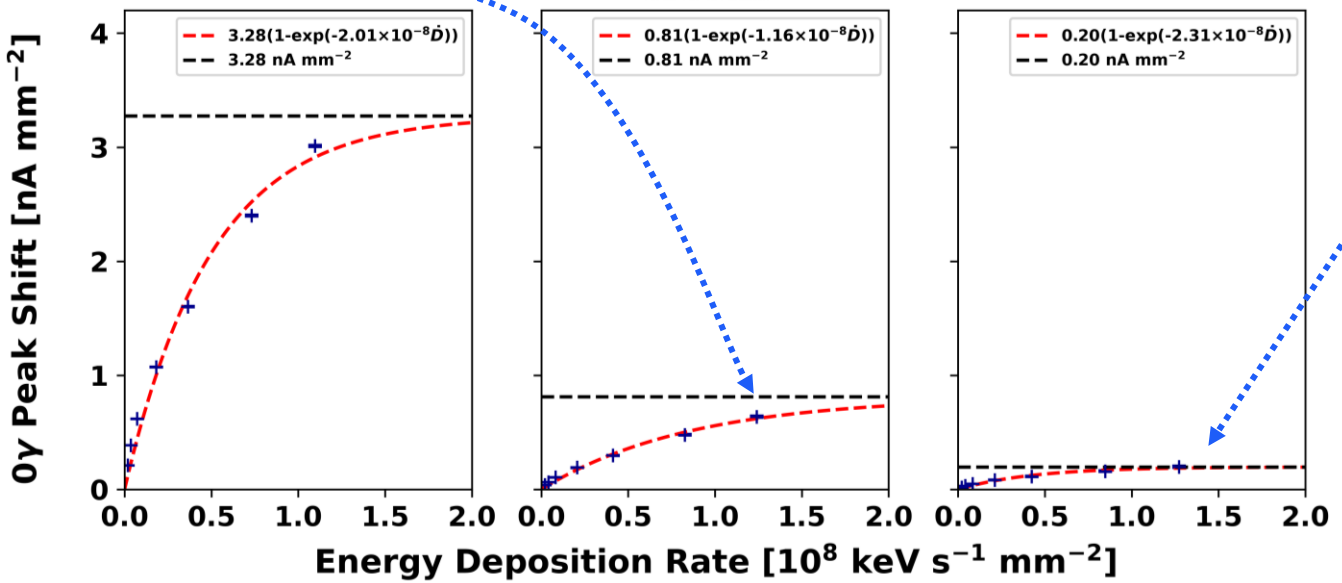

2. N-type LF-CZT cf. p-type HF-CZT
→ fewer anode acceptor traps
+ higher anode barrier
→ lower excess leakage current

Fig 22: Excess leakage current as a function of energy deposition rate for each module.

Positive but expected results on account of device and electrode parameters

Mo fluorescence: bias-induced polarization measurements

- **HF-2 (Ti/Au)** shows **bias-induced polarization** despite improved leakage current
- **300 s Mo fluorescence** (~1.8 × 10^5 ph s^{-1} mm^{-2}):
  - Polarization **within ~10 s for E ≤ 100 V mm^{-1}**
  - Absent in HF-1 (Pt) and LF-1

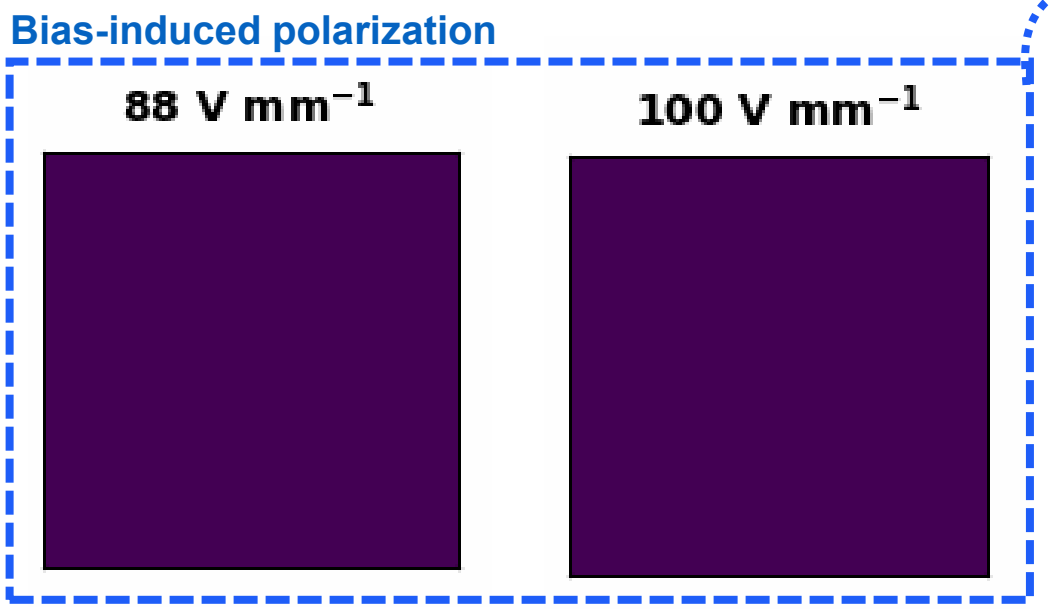

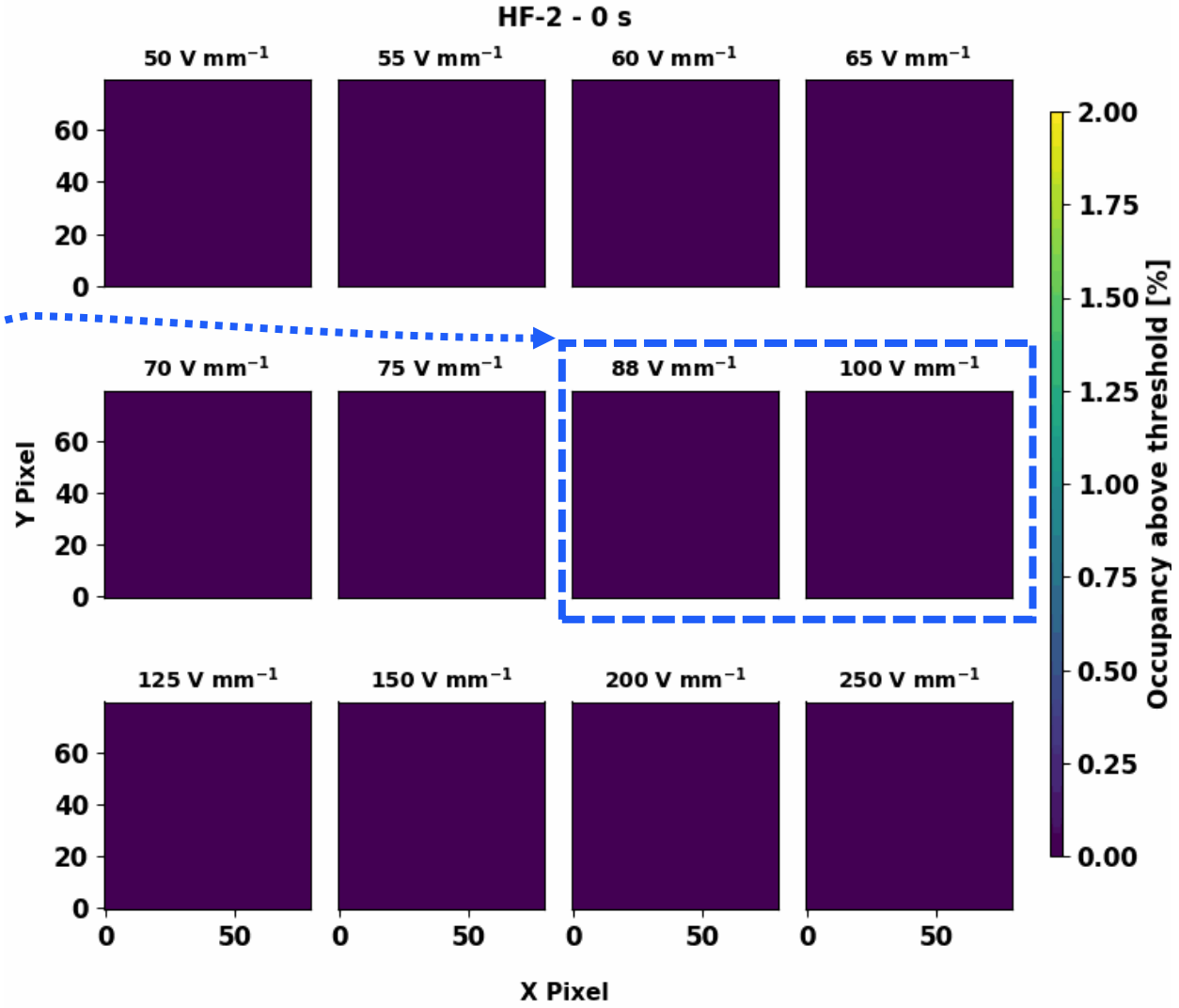

Fig. 23: Comparison of per-pixel occupancy above threshold in HF-CZT: TiPt over time for different electric field strengths.

Science and Technology Facilities Council

Technology

Mo fluorescence: bias-induced polarization measurements

No evident bias-induced polarization within 300 s

Bias-induced polarization evident within 300 s

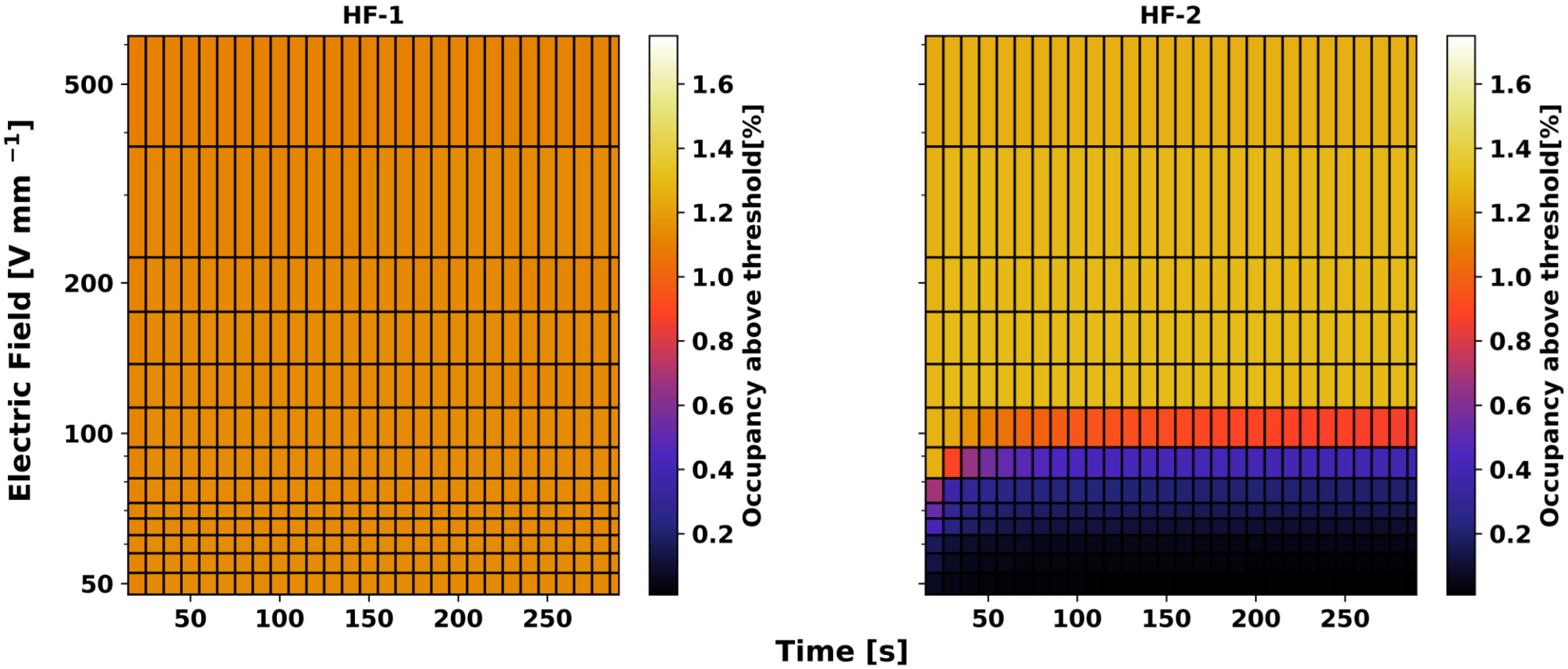

Fig. 24: Comparison of per-pixel occupancy above threshold in HF-1 (Pt) and HF-2 (TiPt) over time for different electric field strengths.

Science and Technology Facilities Council

Technology

Mo fluorescenc

LF-CZT: flux-induced polarization

Figure 10: Difference in ADU between the dark mean count and the mean count of each 100 ms frame, per pixel, at −125 V and increasing time steps, for a) LF-CdZnTe and b) HF-CdZnTe. Underneath each image the lineplot shows the intensity for a row of pixels through the beam area highlighted in white.

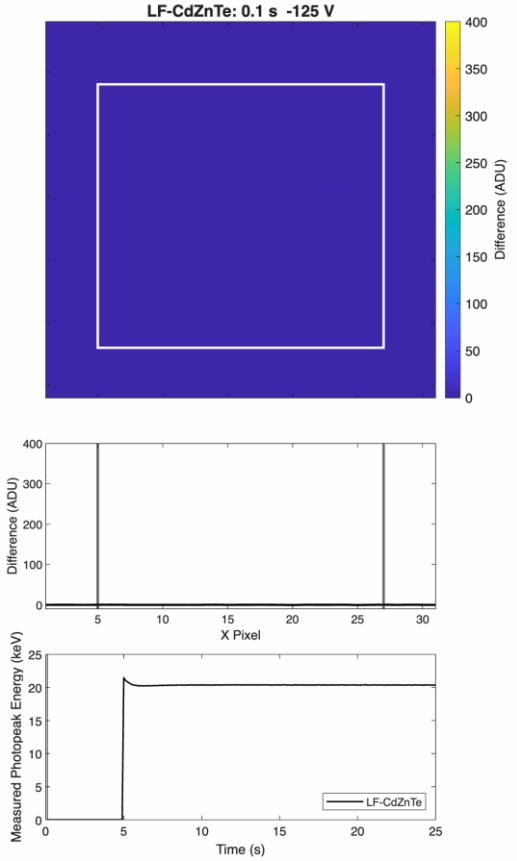

Results from Bishop et al., 2025 [manuscript submitted for publication]

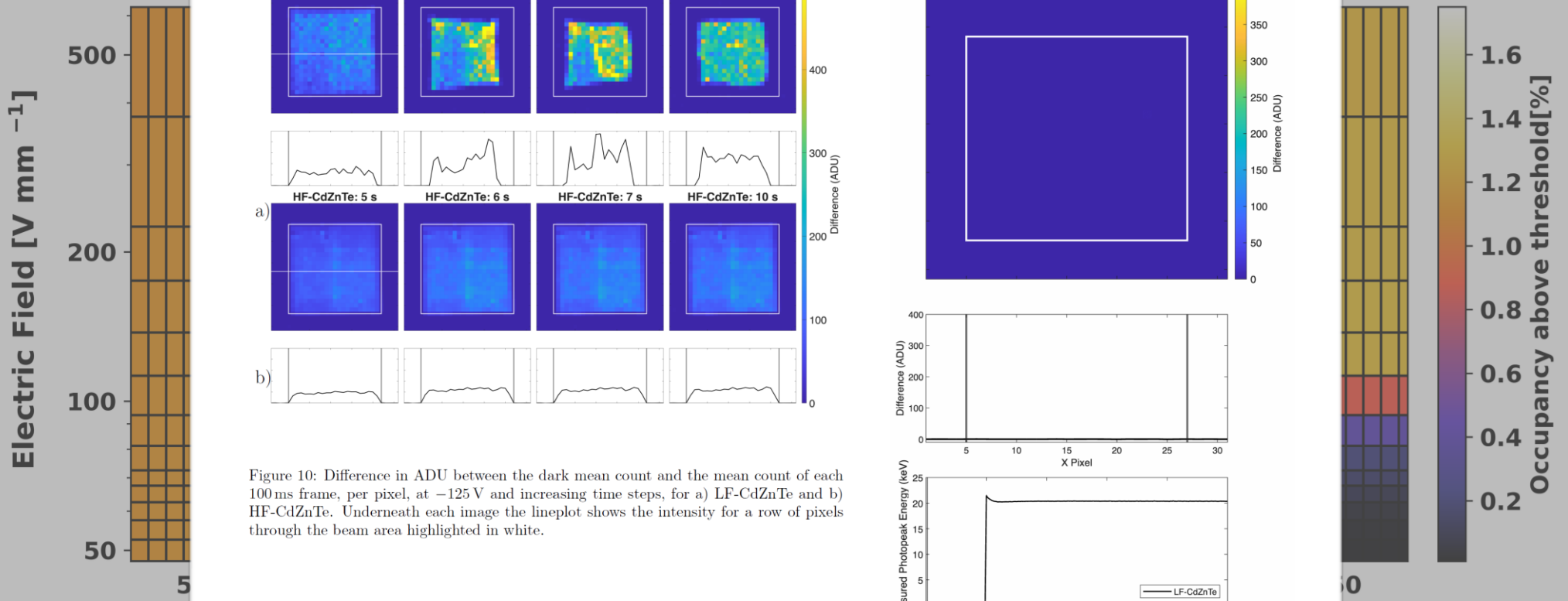

Fig. 24: Co… …engths.

Science and Technology Facilities Council

Technology

Summary

Aim — Characterise HF-CZT performance at X-ray fluxes >10^6 ph s^{-1} mm^{-2}

Outcome — Identification and characterisation of 'excess-leakage-current'

Solution? — HF-CZT: Ti/Au shows a reduced effect but at a cost

Next steps — Wafer-scale measurements to investigate pixel-to-pixel variation

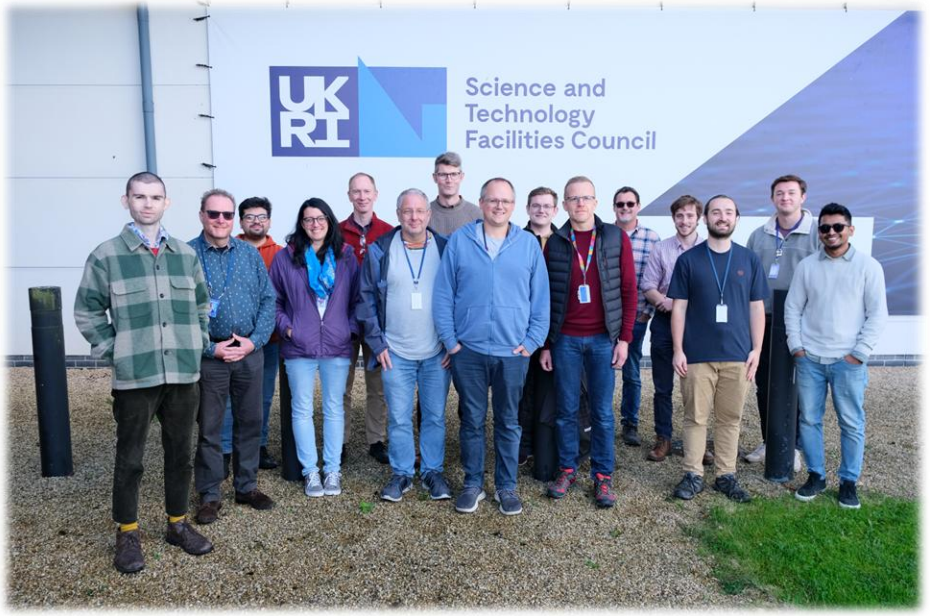

Fig. 25: Members of the $HEXITEC_{MHz}$ team.

For further details, please refer to the following publications:

PAPER • OPEN ACCESS

Characterisation of Redlen HF-CdZnTe at > 10^6 ph s^{-1} mm^{-2} using $HEXITEC_{MHz}$

B.D. Cline[1], D. Banks[1], S. Bell[1], I. Church[1], A. Davis[1], T. Gardiner[1], J. Harris[1], M. Hart[1], L. Jones[1], T. Nicholls[1] Show full author list

Published 24 April 2024 • © 2024 The Author(s)

Journal of Instrumentation, Volume 19, April 2024

Citation B.D. Cline *et al* 2024 *JINST* **19** P04028

DOI: 10.1088/1748-0221/19/04/P04028

PAPER • OPEN ACCESS

Characterisation and quantification of the `Excess-Leakage-Current' effect in Redlen HF-CdZnTe at > 10^6 ph s^{-1} mm^{-2}

B.D. Cline, D. Banks, M. Bishop, A. Davis, J. Harris, M. Hart, S. Knowles, T. Nicholls, J. Nobes, S. Pradeep Show full author list

Published 10 October 2025 • © 2025 The Author(s)

Journal of Instrumentation, Volume 20, October 2025

Citation B.D. Cline *et al* 2025 *JINST* **20** P10021

DOI: 10.1088/1748-0221/20/10/P10021

Science and Technology Facilities Council

Technology

181 MBq ^{241}Am: spectroscopic performance

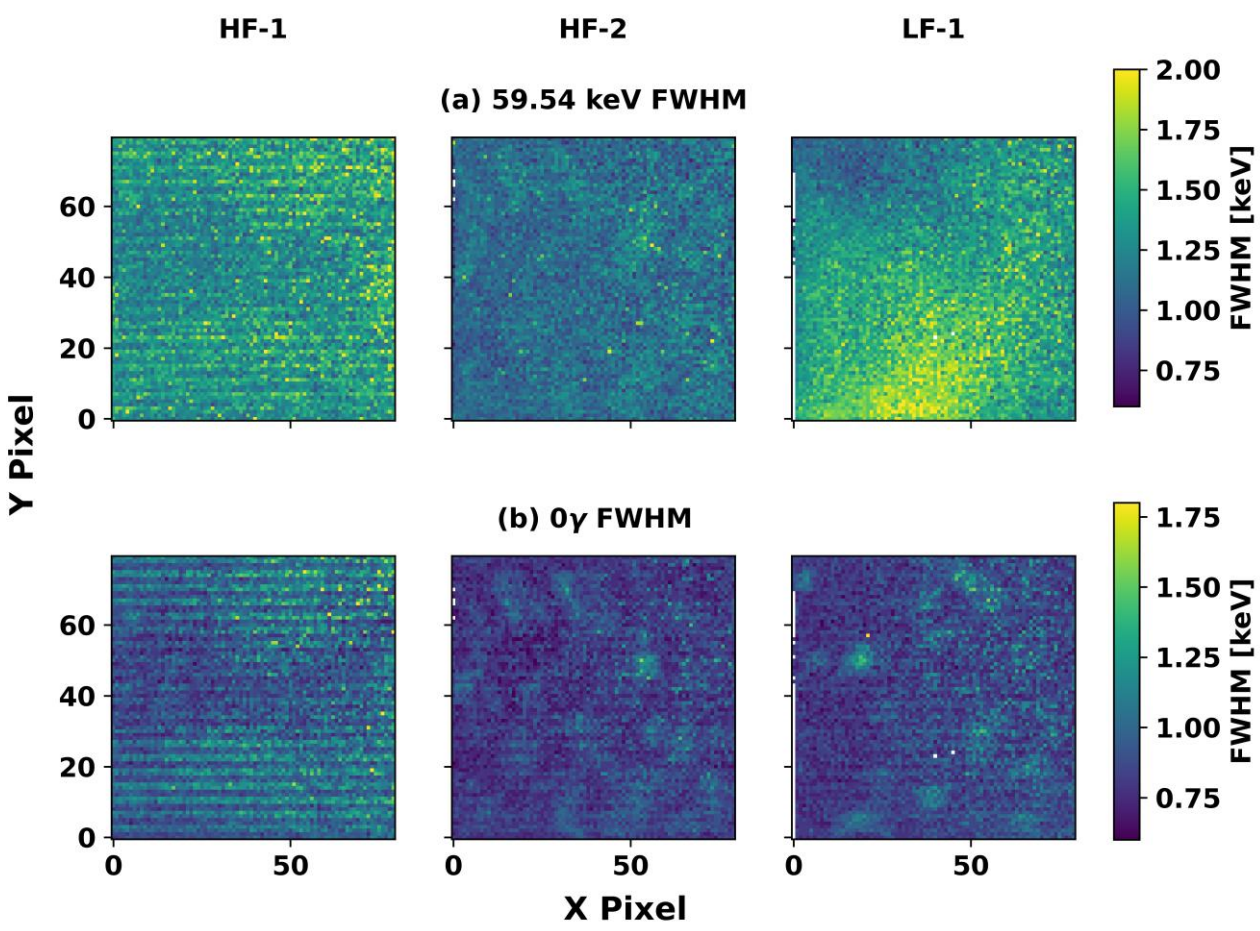

Fig. 26: Maps of the (a) 0γ and (b) 59.54 keV FWHM values for each tested device.

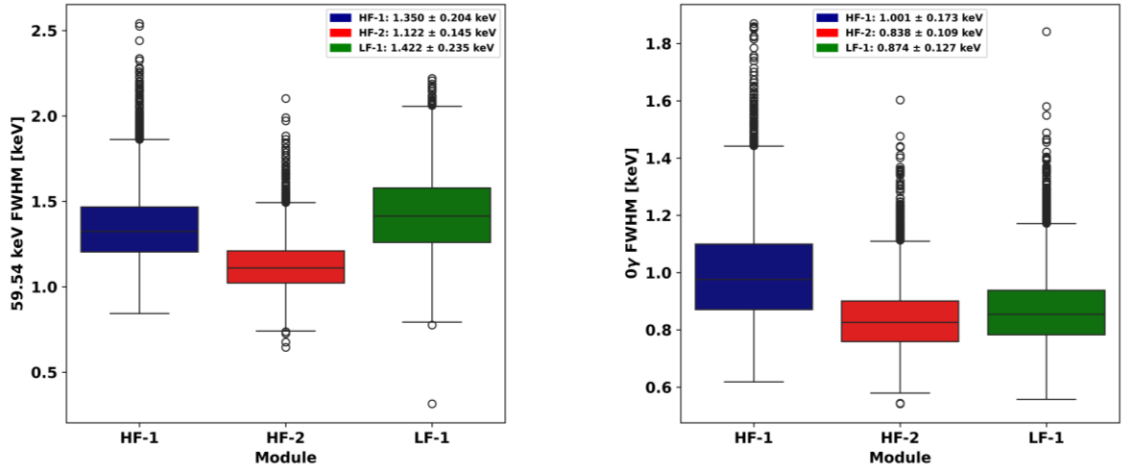

Fig. 27: Boxplots of the (a) 0γ and (b) 59.54 keV FWHM values for each tested device.

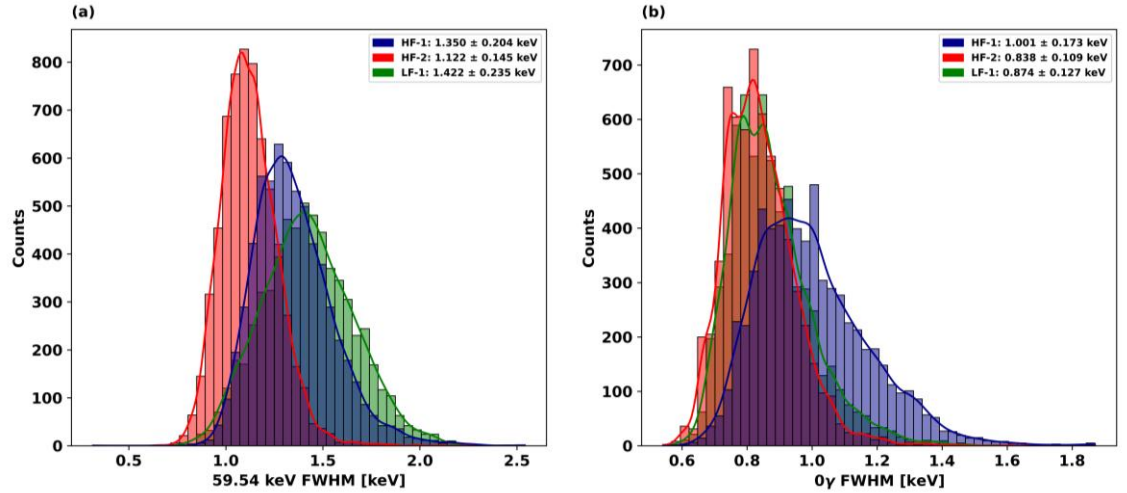

Fig. 28: Histograms of the (a) 0γ and (b) 59.54 keV FWHM values for each tested device.

Science and Technology Facilities Council

Technology

181 MBq ^{241}Am: device uniformity

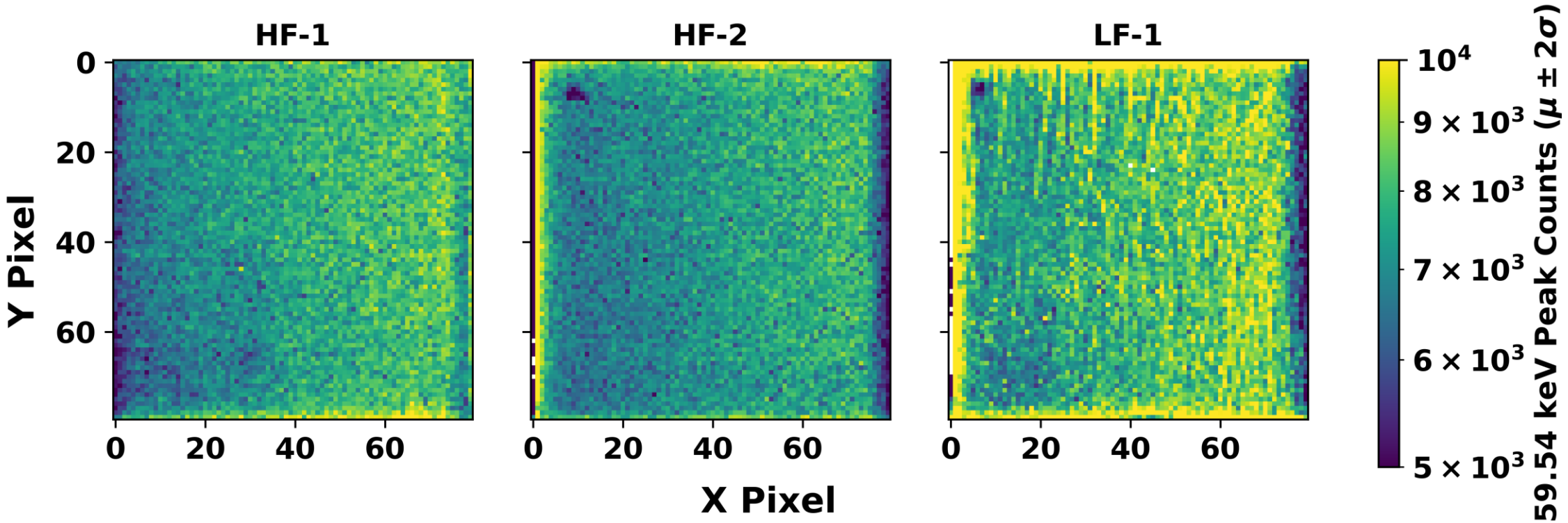

Fig. 29: Maps of the 59.54 keV photopeak counts (μ ± 2σ) for each tested device.

Science and Technology Facilities Council

Technology

In-FPGA Data Correction

- By default, raw 80 × 80 pixel frames are converted in-FPGA into histograms, with each pixel's dark level tracked and corrected before a per-pixel energy calibration is applied. Additional in-FPGA data correction algorithms can be applied and are summarised below:

Tab 3: HEXITEC$_{MHz}$ data correction algorithms.

Data Correction Method	Description
Low-energy thresholding	Counts events where the pixel signal exceeds a low-energy threshold, filtering out sub-threshold charge deposits.
Charge-sharing addition (CSA)	Identifies and sums charge split across neighbouring pixels, recovering the full photon energy and improving detection efficiency.
Charge-sharing discrimination (CSD)	Identifies and reject events where charge is split across neighbouring pixels, reducing low-energy tailing in the spectrum.

Output Data Formats

- Processed histograms can be output in the following forms

Tab 4: HEXITEC$_{MHz}$ data output formats.

Output Format	Description	Data Shape	Data Volume (2048 energy bins)
Per-pixel Energy Spectrum	Single per-pixel energy spectrum output for entire capture	(80, 80, nBins*)	51 MB
Global Energy Spectrum	Single global energy spectrum is output for entire capture	(nBins)	8 kB
Time-resolved Per-Pixel Energy Spectra	Per-pixel energy spectra output at a specified rate for dynamic measurements	(tBins, 80, 80, nBins)	0.51 GB s^{-1} @ 10 Hz
Time-resolved Global Energy Spectra	Global energy spectra output at a specified rate for dynamic measurements	(tBins, nBins)	80 kB s^{-1} @ 10 Hz

**The number of energy bins (nBins) can be set for any bit depth between 7-bit and 12-bit.*

- Raw data can also be captured at a rate of 10 GB s^{-1} for a maximum of 5 s

Data Pipeline

1st Level FPGA: Data Unpacking
Alpha Data ADM-PCIE-9V5 - Low Latency Trading

2nd Level FPGA: Correction & Histogramming
Xilinx Alveo U200

Fast Data Storage
Highpoint SSD7540 NVMe RAID Controller

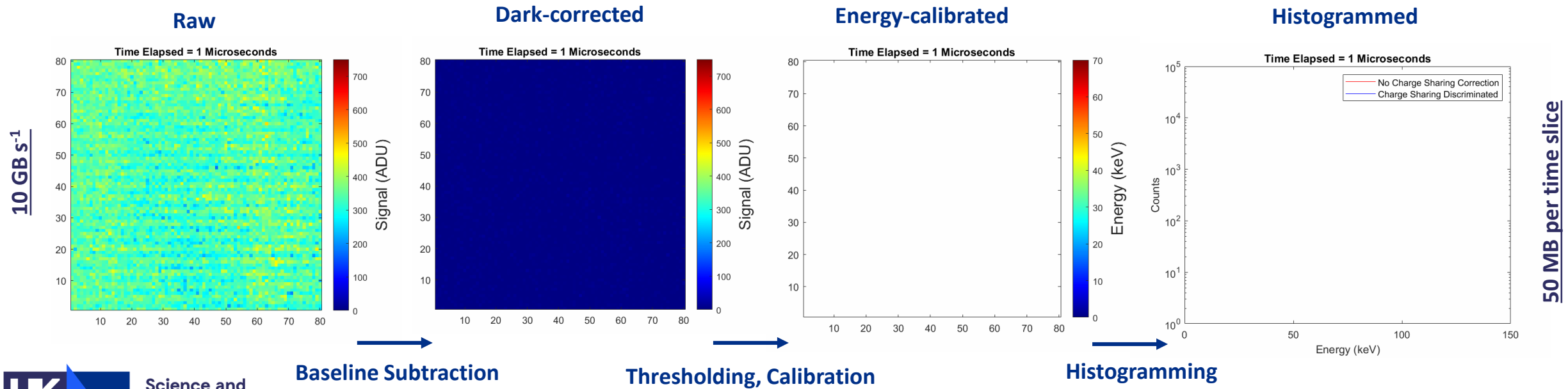

Science and Technology Facilities Council
Technology

Fig. 30: HEXITEC$_{MHz}$ data analysis pipeline.

Triggered acquisitions

- System supports multiple modes for external histogram triggering

Tab 5: HEXITEC$_{MHz}$ triggering modes.

Mode	Description
Step Scan Mode	Collect 1 per-pixel histogram of *n* frames each time a trigger is received
Continuous Mode	Continuously assign frames to the current per-pixel histogram until a new trigger is received
Burst Mode	Collect *t* per-pixel histograms of *n* frames each time a trigger is received